

Plastic Burning Particulate Matter as a Source of Environmentally Persistent Free Radicals and Reactive Oxygen and Chlorine Species

Rizana Salim^{1,2,3}, Sukriti Kapur³, Meredith Schervish³, Lena Gerritz³, Kasey C. Edwards³, Luis Ruis-Armenta³, Emil Varghese^{1,2}, Raghunathan Ravikrishna⁴, Sergey A. Nizkorodov³, Sachin S. Gunthe^{1,2,*}, Manabu Shiraiwa^{3,*}

¹ Centre for Atmospheric and Climate Sciences (CACCS), Indian Institute of Technology Madras, Chennai 600036, India

² Environmental Engineering division, Department of Civil Engineering, Indian Institute of Technology Madras, Chennai 600036, India

³ Department of Chemistry, University of California, Irvine, 92697, United States

⁴ Department of Chemical Engineering, Indian Institute of Technology Madras, Chennai 600036, India

Email: m.shiraiwa@uci.edu, s.gunthe@iitm.ac.in

Supplementary notes

This supplementary file contain:

1. Supplementary notes
2. Supplementary figures, S1- S12
3. Supplementary tables, 1-3

Additional information on kinetic modelling

To achieve better agreement between the model and measurements, a total •OH reactivity with organics of $1.15 \times 10^{15} \text{ s}^{-1}$, $5.75 \times 10^{14} \text{ s}^{-1}$, and $5.75 \times 10^{14} \text{ s}^{-1}$ were assumed for HDPE, PVC and PS, respectively. As the model underestimated the OP-OH values for LDPE and PET without the •OH reaction with organics, the reactivity of •OH toward organics in these plastics needs to be below $\sim 1 \times 10^{12} \text{ s}^{-1}$ so that it is not competitive with the OP+TPT reaction. The broad implementation of one organic+OH reaction is intended to cover the reactivity of a variety of organic species potentially present in the plastic burning PM, including plasticizers. Without this reaction present all the simulated OP-OH values are still within an order of magnitude of the measured values, providing great evidence for the •OH production mechanism used here explaining the •OH formation in these plastics.

Without inclusion of the reaction of OH with organics, only the OP-OH of PET is simulated to be within one standard deviation of the OP-OH measurements (Figure S11). LDPE is underestimated as discussed previously and HDPE is slightly overestimated. OP-OH in PVC and PS are greatly overestimated due to the high values of all input species in these plastics and minimal competition for OH without the organic reaction. The overestimation is by less than a factor of 4 for both plastics.

Figure S12 shows correlation plots between the simulated OP-OH and each of the model inputs. With only five data points, these correlations should not be interpreted broadly, but they provide useful insight into the key parameters controlling OH formation in these systems. The strongest correlation is observed for the total metals with Ni and Sb both showing moderate correlations with simulated OP-OH individually, as Fenton chemistry is critical for producing OH. A strong correlation is also seen for PAHs, which used as a proxy for quinones lead to formation of EPFRs. The EPFR concentration is not correlated with the simulated OP-OH as the EPFR production ability of each PM is better represented with the PAH concentration. No correlation is seen for simulate OP-OH and HOCl as it is likely in excess.

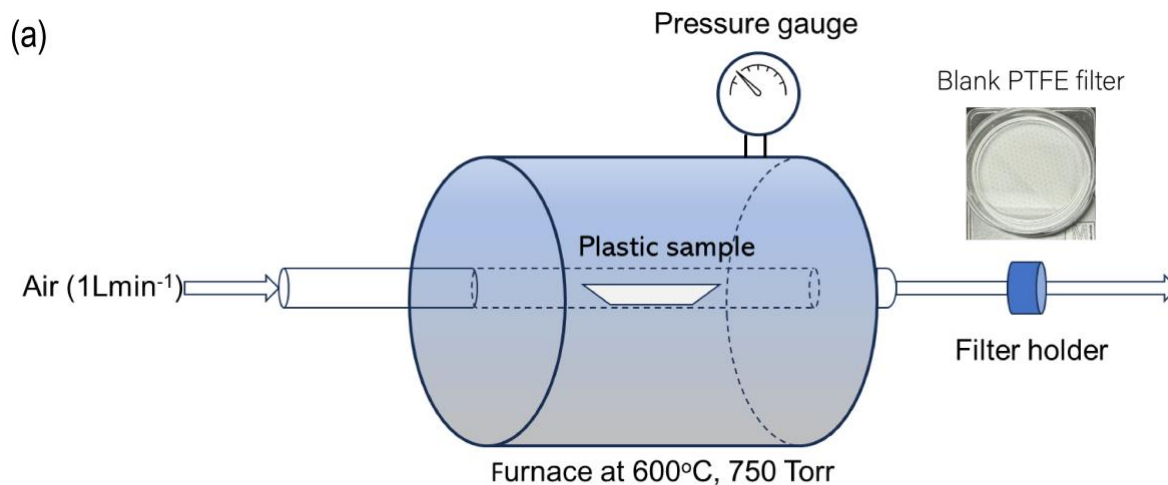
Of note is that the OP-OH is most overestimated for PVC and PS plastic burning PM (without the organic+OH reaction considered) and these two types of plastic burning PM have the highest total metal content (considering only the metals included in the model). While we assume all metals to be completely water soluble, accounting for partial water solubility of metals may lead to better model representation and measurements of metal solubility would be helpful in future studies.

HOCl calibration curve

The calibration curve is fitted using a four-parameter logistic model². It uses the following four parameters:

1. **Min:** the point of smallest response; can be baseline response, control or response when treatment concentration is zero.
2. **Max:** the point of greatest response
3. **X50:** the dose at which the curvature of the response line changes; where the rate of change switches signs (Inflection point)
4. **Hill coefficient:** the slope of the curve at the inflection point

$$Y = Min + \frac{Max - Min}{1 + \left(\frac{X}{X50}\right)^{Hill\ coefficient}}$$



(b)



Figure S1. PM generation from the different plastics using tube furnace. **a**, Schematic diagram of the tube furnace used in the laboratory to generate the particulate matter by the controlled combustion of five different types of plastics- low-density polyethylene (LDPE), high-density polyethylene (HDPE), polyvinyl chloride (PVC), polystyrene (PS) and polyethylene terephthalate (PET) using a chamber equipped with a 2.5 cm diameter quartz tube and a Thermolyne 21135 tube furnace. An exemplary image of blank filter is also shown. **b**, Exemplary images of the charred residue from the furnace post-combustion. Black charred residue results from burning PS, PET, and PVC, while lighter residue is produced from burning LDPE and HDPE.

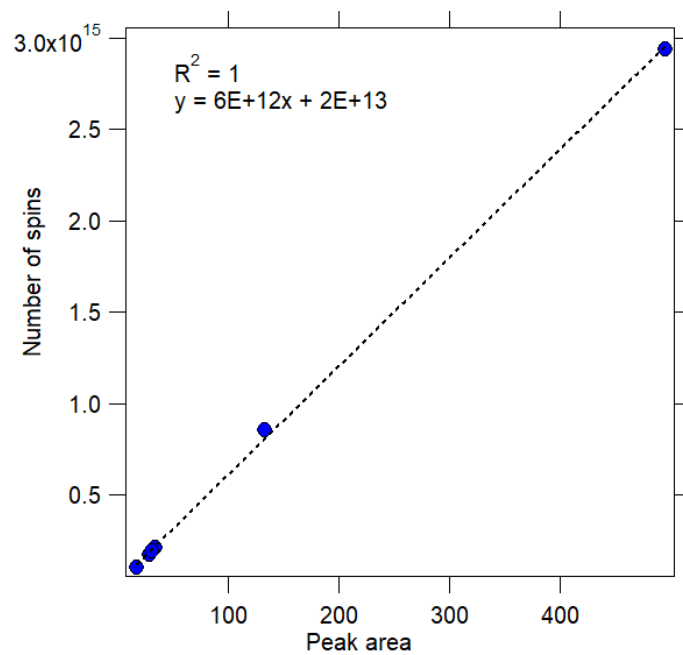


Figure S2. TEMPOL calibration curve. TEMPOL calibration curve is prepared using TEMPOL standards with concentrations ranging from 1 to 200 μM based on the peak area of the EPFR signal and their corresponding number of spins. The equation of TEMPOL calibration curve is used for quantifying the environmentally persistent free radicals.

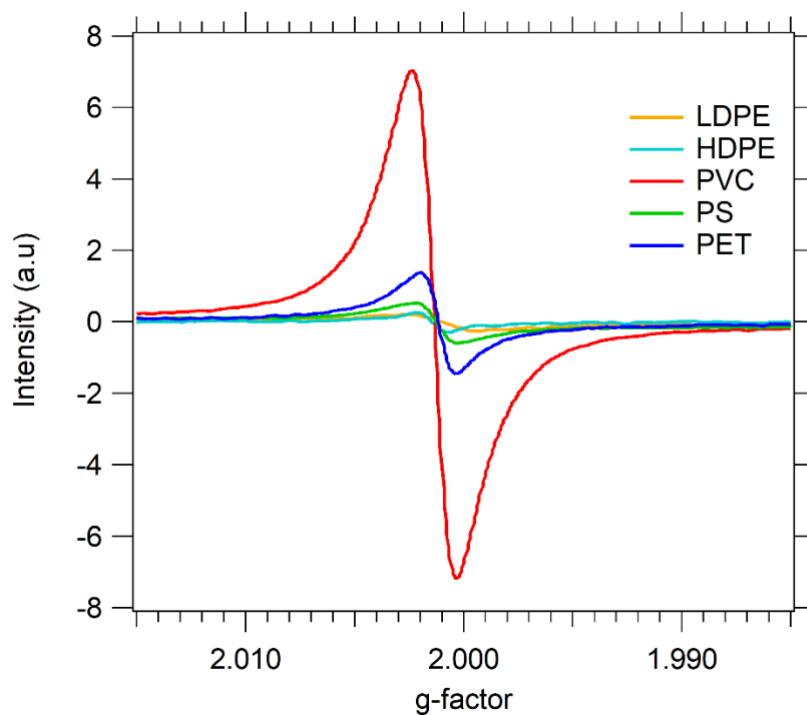


Figure S3. Environmentally persistent free radicals. Electron paramagnetic resonance (EPR) spectra of EPFRs of particulate matter generated by controlled combustion of LDPE, HDPE, PVC, PS and PET. Each type of plastic is colour-coded differently.

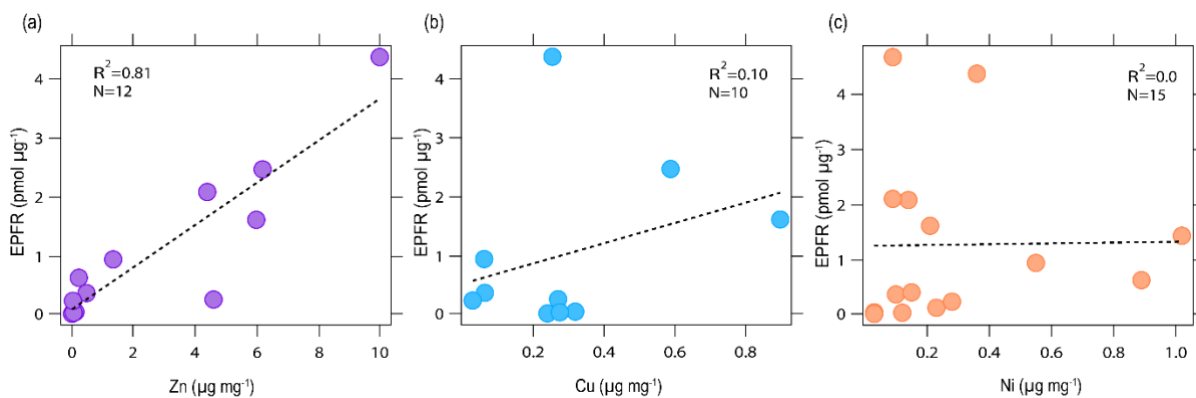


Figure S4. Scatter plot of transition metals with EPFRs. **a** Zn, **b** Cu and **c** Ni with EPFRs in particulate matter generated by burning different plastics. Although, there were ideally 15 data points, some were excluded since the metal concentration fell below the detection limit.

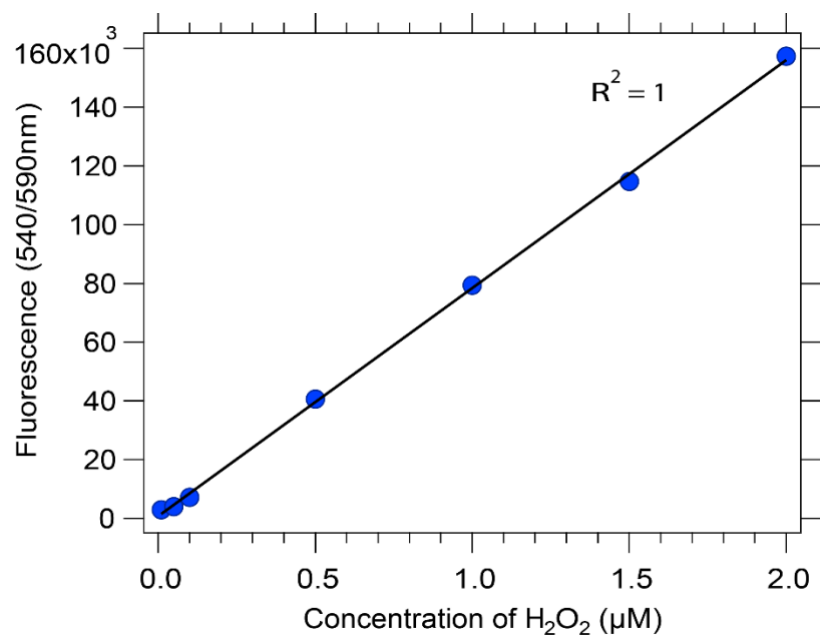


Figure S5. H₂O₂ calibration curve. Calibration curve prepared using H₂O₂ standards ranging from 0.05 to 2.0 µM using a spectrofluorophotometer at excitation and emission wavelengths of 540 nm and 590 nm.

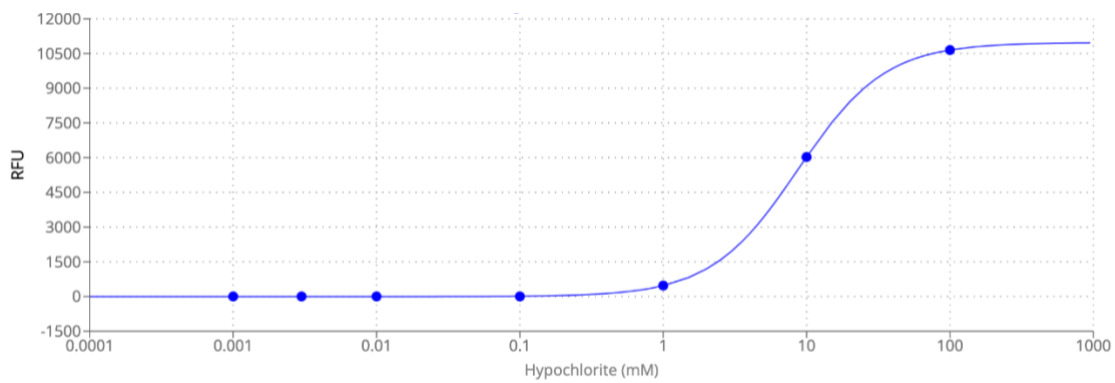


Figure S6. HOCl calibration curve. Calibration was performed using HOCl standard solutions, with concentrations from 0.001-100 mM and fluorescence was measured at Ex/Em of 520/590 nm.

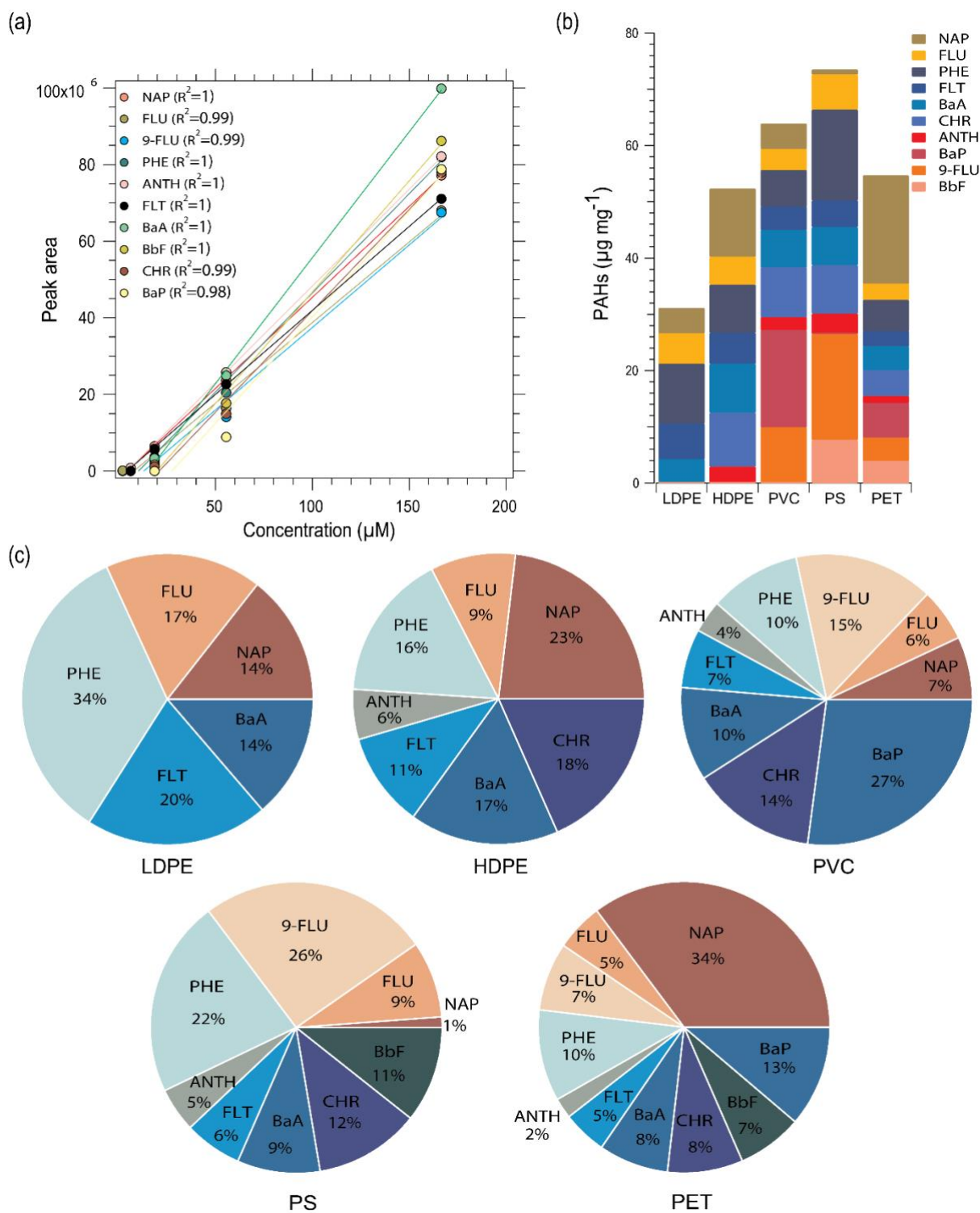


Figure S7. PAH analysis. **a**, Calibration curve of the 10 PAHs analysed using gas chromatography/mass spectrometry including the R² values for each individual calibration curve. **b**, Stacked bar graph of concentration of 10 PAHs, with each PAHs colour-coded differently. **c**, Pie chart illustrating the relative concentration of PAHs in the plastic samples. The PAHs illustrated in the figures are named as follows: Naphthalene (NAP), Fluorene (FLU), Phenanthrene (PHE), Anthracene (ANTH), 9-Fluorenone (9-FLU), Fluoranthene (FLT), Benzantracene (BaA), Chrysene (CHR), Benzo[b]fluoranthene (BbF), and Benzo[a]pyrene (BaP).

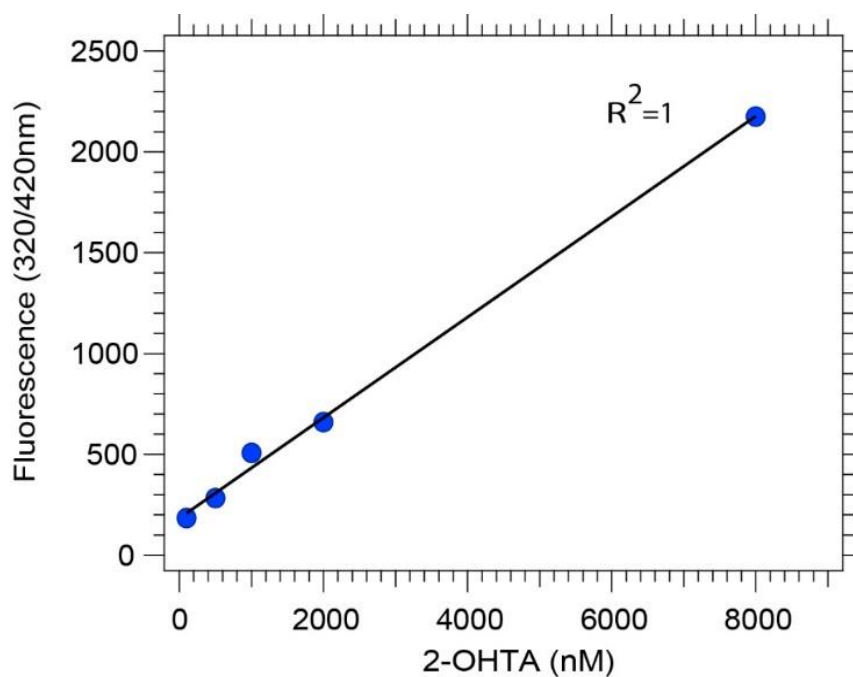


Figure S8. 2-OHTA calibration curve. A calibration curve for 2-OHTA ranging from 100-8000 nM, used for quantifying OH radical formation in OP-OH in surrogate lung fluid (SLF). Calibration is performed using 2-OHTA standards at varying concentrations and measuring the fluorescence at 320/420nm.

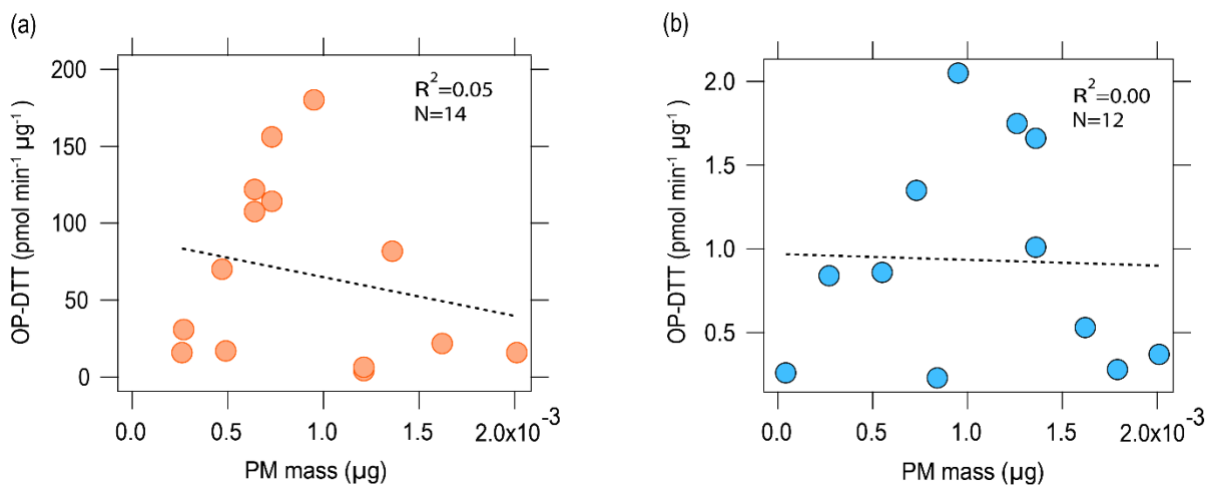


Figure S9. Scatter plots of OP with PM mass. Scatter plots of OP-DTT and OP-OH with PM mass. There were ideally 15 data points, some were excluded as OP fall below the detection limit. No correlation is seen for OP with PM mass.

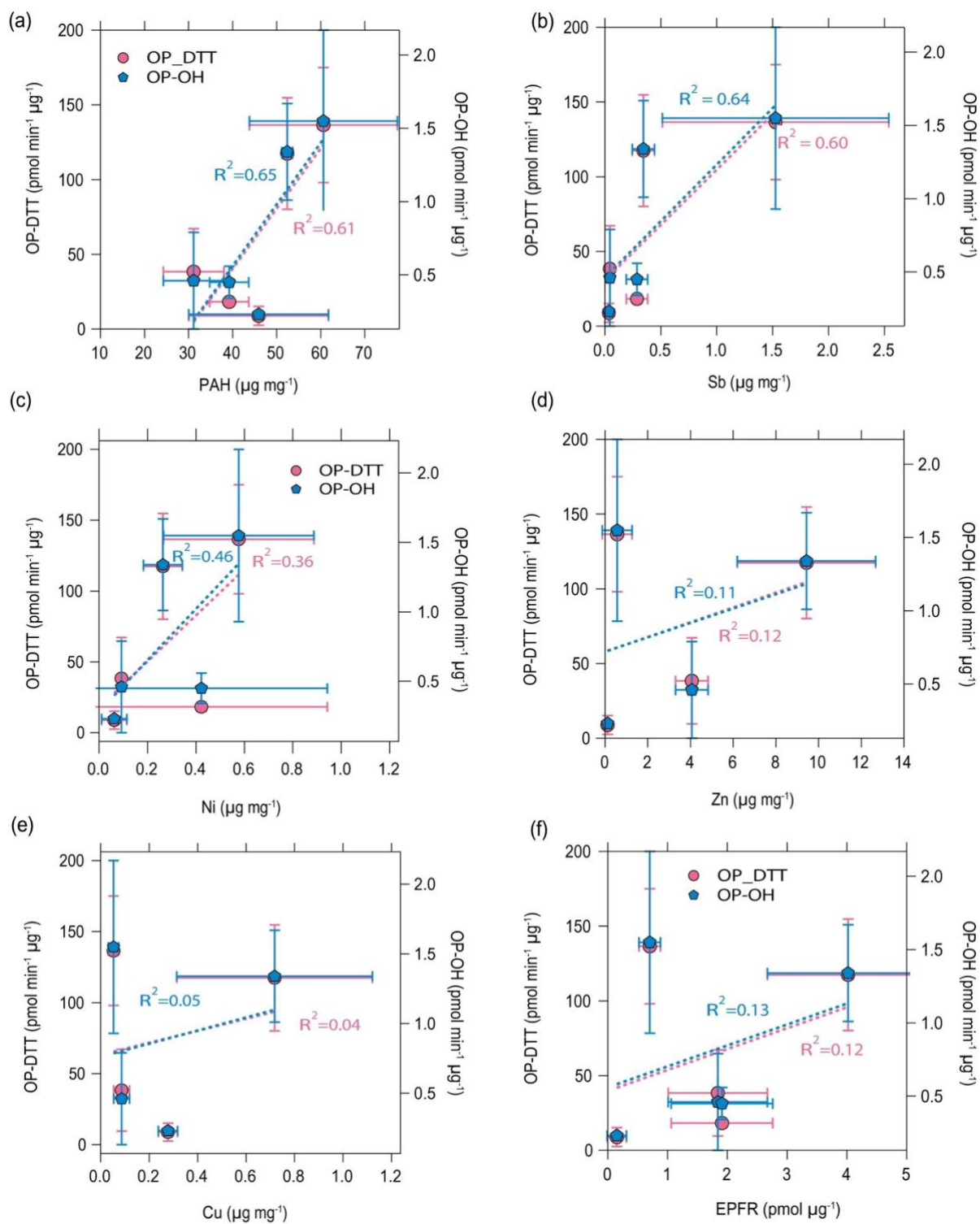


Figure S10. Scatter plot of OP with total PAHs, metals and EPFR. Scatter plot of OP-DTT and OP-OH with (a) total PAHs, (b) Sb, (c) Zn, (d) Cu and (e) Ni and (f) EPFRs. Each value is an average of three measurements, with the error bars represents one standard deviation. The results of OP-DTT and OP-OH are colour coded differently.

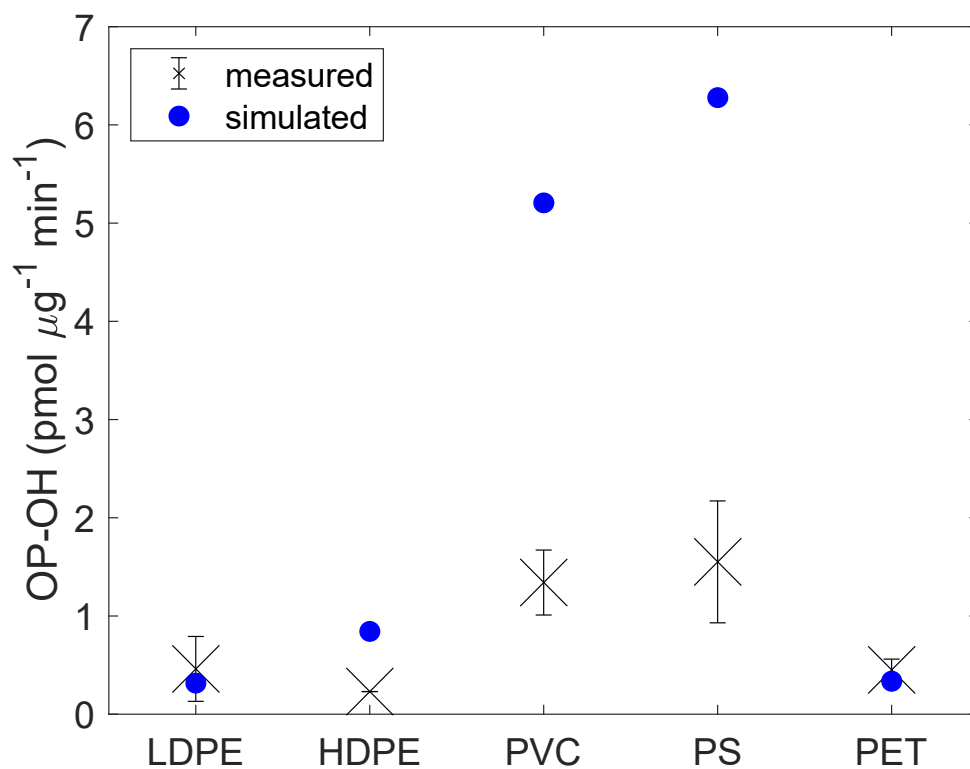


Figure S11. Simulation of OP-OH. Simulation of the OP-OH (blue dots) based on the mechanism given in the SI compared to measurements of OP-OH (black crosses) in the different plastic types. Unlike Figure 4b, the modelled results shown here do not account for the reaction of OH radicals with organic compounds, and simulated OP-OH is particularly overestimated for PVC, PS and HDPE. Error bars on each measurement represent one standard deviation.

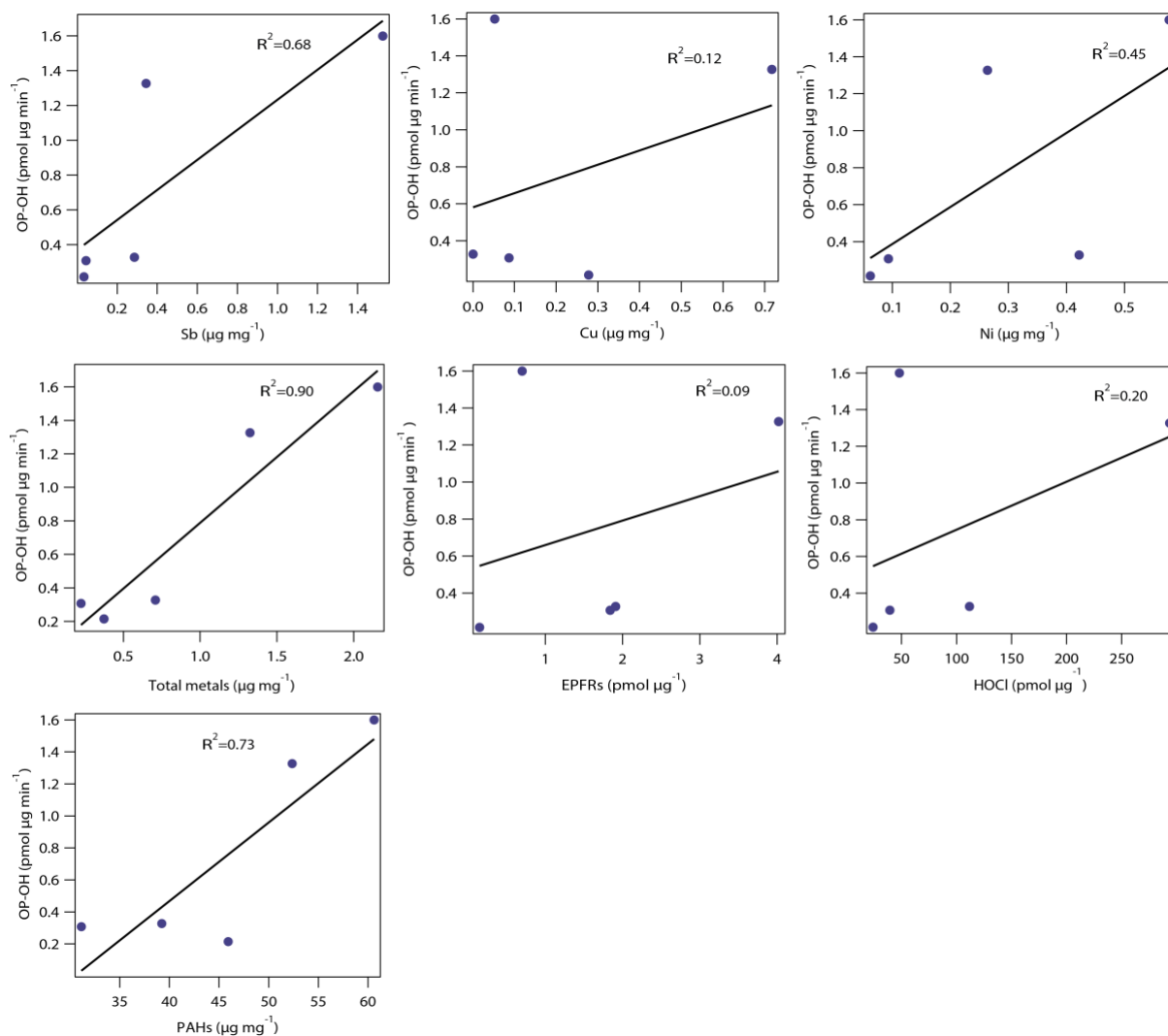


Figure S12. Correlations of input variables with simulate OP-OH. Correlation plots of Sb, Cu, Ni, total metals, EPFRs, HOCl and PAHs with simulate OP-OH values. Linear fits are shown in black lines with R² values.

Table S1. The concentration of PAHs in the plastic burning PM and their diagnostic ratios. The PAHs analysed and quantified for the different types of plastic burning PM are given, with values expressed in $\mu\text{g mg}^{-1}$. The PAH diagnostic ratios can be used for source apportionment and a ratio of ANTH/(ANTH+PHE) < 0.1 signifies petrogenic origins, while values > 0.1 suggest pyrogenic sources. Similarly, a BaA/(BaA+CHR) ratio < 0.2 indicates petrogenic sources, ratios > 0.35 point to pyrolytic origins, and values between 0.2-0.35 suggest a mixture of petroleum and combustion sources¹.

PAHs	LDPE	HDPE	PVC	PS	PET
NAP	4.49	12.10	4.47	0.87	19.25
FLU	5.43	4.95	3.76	6.27	2.89
9-FLU			9.89	18.83	4.14
PHE	10.63	8.58	6.50	16.11	5.55
ANTH		2.91	2.29	3.62	1.25
FLT	6.32	5.51	4.14	4.72	2.69
BaA	4.27	8.66	6.66	6.77	4.23
CHR		9.63	8.84	8.61	4.57
BbF				7.68	3.98
BaP			17.31	0.00	6.14
PAH diagnostic ratios					
ANTH/(ANTH+PHE)	-	0.25	0.26	0.18	0.18
BaA/(BaA+CHR)	-	0.47	0.43	0.44	0.48

Table S2. Chemical reactions and rate constants included in the model.

Reaction	Rate Constant (cm ³ s ⁻¹ for bimolecular reactions and s ⁻¹ for unimolecular reactions)	Reference
HQ + Q → 2SQ + 2H ⁺	9.63×10 ⁻²⁰	3
2SQ + 2H → HQ + Q	1.33×10 ⁻¹³	
HQ + OH → HQOH	1.99×10 ⁻¹¹	
Q + OH → QOH	1.1×10 ⁻¹¹	
HOCl + O ₂ ⁻ → OH + O ₂ + Cl ⁻	1.25×10 ⁻¹⁴	
HOCl + HQ → Q + Cl ⁻	3.6×10 ⁻²⁰	
HOCl + SQ → Q + HOCl ⁻	3.6×10 ⁻²⁰	
HOCl ⁻ → OH + Cl ⁻	1.01×10 ⁻¹¹	
OH + Cl ⁻ → HOCl	7.14×10 ⁻¹²	
O ₂ ⁻ + O ₂ ⁻ → H ₂ O ₂ + O ₂	2.66 × 10 ⁻¹²	
HO ₂ → O ₂ ⁻ + H ⁺	226000 s ⁻¹	
O ₂ ⁻ + OH → O ₂ + OH ⁻	1.3×10 ⁻¹¹	
HQ + O ₂ → O ₂ ⁻ + SQ	1.66×10 ⁻²⁸	
O ₂ ⁻ + SQ + 2H ⁺ → HQ + O ₂	1.66×10 ⁻¹⁴	
H ₂ O ₂ + OH → H ₂ O + HO ₂	5.48×10 ⁻¹⁴	
OH + OH → H ₂ O ₂	8.64×10 ⁻¹²	
OH + HO ₂ → H ₂ O + O ₂	1.18×10 ⁻¹¹	
HO ₂ + HO ₂ → H ₂ O ₂ + O ₂	1.38×10 ⁻¹⁵	
H ₂ O ₂ + HO ₂ → H ₂ O + O ₂ + OH	5×10 ⁻²¹	
H ⁺ + O ₂ ⁻ → HO ₂	1×10 ⁻¹¹	
HO ₂ + O ₂ ⁻ → H ₂ O ₂ + OH ⁻ + O ₂	1.7×10 ⁻¹³	
SQ + O ₂ → Q + O ₂ ⁻	4.63×10 ⁻¹³	
SQ + O ₂ ⁻ → Q + H ₂ O ₂	3.28×10 ⁻¹²	
Cu ⁺ + H ₂ O ₂ → Cu ³⁺ + 2OH ⁻	4.95×10 ⁻¹⁹	
Cu ⁺ + O ₂ → O ₂ ⁻ + Cu ²⁺	6.89×10 ⁻²⁰	
Cu ⁺ + O ₂ ⁻ → Cu ²⁺ + H ₂ O ₂	5.79×10 ⁻¹⁵	
Cu ⁺ + H ₂ O ₂ → Cu ³⁺ + OH ⁻ + OH	2.39×10 ⁻²⁰	
Cu ²⁺ + H ₂ O ₂ → Cu ⁺ + 2OH	2.39×10 ⁻²⁰	
Cu ⁺ + Cu ³⁺ → 2Cu ²⁺	5.81×10 ⁻¹²	
Cu ²⁺ + H ₂ O ₂ → Cu ⁺ + O ₂ ⁻ + 2H ⁺	3.8×10 ⁻²⁴	
Cu ²⁺ + O ₂ ⁻ → Cu ⁺ + O ₂	8.32×10 ⁻¹²	
HO ₂ + Cu ²⁺ → H ⁺ + Cu ⁺ + O ₂	1.55×10 ⁻¹¹	
HO ₂ + Cu ⁺ → H ₂ O ₂ + Cu ²⁺ + OH ⁻	2.27×10 ⁻¹²	
Cu ⁺ + O ₂ → Cu ²⁺ + O ₂ ⁻	6.9×10 ⁻²⁰	
Sb ³⁺ + H ₂ O ₂ → Sb ⁵⁺ + OH + OH ⁻	2.5×10 ⁻²⁰	5
Sb ³⁺ + OH → Sb ⁴⁺ + OH ⁻	1.4×10 ⁻¹¹	
Ni ²⁺ + H ₂ O ₂ → Ni ³⁺ + OH + OH ⁻	2.39×10 ⁻²⁰	
AscH + O ₂ ⁻ + H ⁺ → Asc ⁻ + H ₂ O ₂	5.13×10 ⁻¹⁷	4
Asc ⁻ + Asc ⁻ + H ⁺ → AscH	5×10 ⁻¹⁶	
OH + AscH → H ₂ O + Asc ⁻	1.8×10 ⁻¹¹	
Q + AscH → SQ + Asc ⁻	1.21×10 ⁻²⁰	

HQ + AscH → SQ + Asc ⁻	9.63×10 ⁻¹⁹	
AscH + Cu ²⁺ → Cu ⁺ + Asc ⁻	1.37× 10 ⁻¹⁸	
UA + OH → Product	1.2×10 ⁻¹¹	6
GSH + OH → Product	1.7×10 ⁻¹¹	
AscH + GS → GSH + Asc ⁻	1×10 ⁻¹²	
AscH + UA → UAH + Asc ⁻	1.7×10 ⁻¹⁵	
UAH ⁻ + GS → GSH + UA	5×10 ⁻¹⁴	
Organic + OH → Prod	1.15×10 ⁻¹²	4,6
OH + TPT → 2-OHTA	6.21×10 ⁻¹²	3,4

Table S3. List of abbreviations.

PM	Particulate matter
OP	Oxidative potential
DTT	Dithiothreitol
ROS	Reactive oxygen species
RCS	Reactive chlorine species
DNA	Deoxyribonucleic Acid
HULIS	Humic-like substances
LDPE	Low-density polyethylene
HDPE	High-density polyethylene
PVC	Polyvinyl chloride
PS	Polystyrene
PET	Polyethylene terephthalate
PAH	Polycyclic aromatic hydrocarbons
NAP	Naphthalene
FLU	Fluorene
9-FLU	9-Fluorenone
PHE	Phenanthrene
ANTH	Anthracene
FLT	Fluoranthene
CHR	Chrysene
BaA	Benzanthracene
BbF	Benzo[b]fluoranthene
BaP	Benzo[a]pyrene
BSTFA	N,O-Bis(trimethylsilyl)trifluoroacetamide
US EPA	United states environmental protection agency
UV	Ultraviolet
EPR	Electron paramagnetic resonance
EPFR	Environmentally persistent free radicals
BMPO	5-tert-Butoxycarbonyl-5-methyl-1-pyrroline-N-oxide
SQ	Semiquinone
COPD	Chronic obstructive pulmonary disorder
WUI	Wildland urban interface
PTFE	Polytetrafluoroethylene
PBS	Phosphate buffered saline
SOA	Secondary organic aerosols

ICP - MS	Inductively coupled plasma mass spectrometry
GC - MS	Gas chromatography mass spectrometry
DCM	Dichloromethane
TCA	Trichloroacetic acid
DNTB	5,5'-dithiobis(2-nitrobenzoic acid)
SLF	Surrogate lung fluid
TPT	Disodium terephthalate
OHTA	2-hydroxy terephthalic acid

References

1. Yunker, M. B. *et al.* PAHs in the Fraser River basin: a critical appraisal of PAH ratios as indicators of PAH source and composition. *Organic Geochemistry* **33**, 489–515 (2002).
2. AAT Bioquest, Inc. Four Parameter Logistic (4PL) Curve Calculator. (2024).
3. Liou, S.-Y. & Dodd, M. C. Evaluation of hydroxyl radical and reactive chlorine species generation from the superoxide/hypochlorous acid reaction as the basis for a novel advanced oxidation process. *Water Research* **200**, 117142 (2021).
4. Lakey, P. S. J. *et al.* Chemical exposure-response relationship between air pollutants and reactive oxygen species in the human respiratory tract. *Sci Rep* **6**, 32916 (2016).
5. Rong, Q., Zhang, C., Ling, C., Lu, D. & Jiang, L. Mechanism of extracellular electron transport and reactive oxygen mediated Sb(III) oxidation by *Klebsiella aerogenes* HC10. *Journal of Environmental Sciences* **147**, 11–21 (2025).
6. Tong, H. *et al.* Reactive Oxygen Species Formed by Secondary Organic Aerosols in Water and Surrogate Lung Fluid. *Environ. Sci. Technol.* **52**, 11642–11651 (2018).